NANO · MICRO small
www.small-journal.com

# Nanoglass–Nanocrystal Composite—a Novel Material Class for Enhanced Strength–Plasticity Synergy

*Shyam Katnagallu,* Ge Wu, Shiv Prakash Singh, Sree Harsha Nandam, Wenzhen Xia, Leigh T. Stephenson, Herbert Gleiter, Ruth Schwaiger, Horst Hahn, Michael Herbig, Dierk Raabe, Baptiste Gault,* and Shanoob Balachandran*

**The properties of a material can be engineered by manipulating its atomic and chemical architecture. Nanoglasses which have been recently invented and comprise nanosized glassy particles separated by amorphous interfaces, have shown promising properties. A potential way to exploit the structural benefits of nanoglasses and of nanocrystalline materials is to optimize the composition to obtain crystals forming within the glassy particles. Here, a metastable Fe-10 at% Sc nanoglass is synthesized. A complex hierarchical microstructure is evidenced experimentally at the atomic scale. This bulk material comprises grains of a $Fe_{90}Sc_{10}$ amorphous matrix separated by an amorphous interfacial network enriched and likely stabilized by hydrogen, and property-enhancing pure-Fe nanocrystals self-assembled within the matrix. This composite structure leads a yield strength above 2.5 GPa with an exceptional quasi-homogeneous plastic flow of more than 60% in compression. This work opens new pathways to design materials with even superior properties.**

Dr. S. Katnagallu, Dr. G. Wu, Dr. L. T. Stephenson, Dr. M. Herbig, Prof. D. Raabe, Dr. B. Gault, Dr. S. Balachandran
Department of Microstructure Physics and Alloy Design
Max-Planck-Institut für Eisenforschung GmbH
Düsseldorf 40237, Germany
E-mail: b.gault@mpie.de

Dr. S. Katnagallu, Dr. S. P. Singh, Dr. S. H. Nandam, Prof. H. Gleiter, Prof. H. Hahn
Institute of Nanotechnology
Karlsruhe Institute of Technology (KIT)
Karlsruhe 76021, Germany
E-mail: shyam.katnagallu@kit.edu

Dr. W. Xia
Department of Structure and Nano-Micromechanics of Materials
Max-Planck-Institut für Eisenforschung GmbH
Düsseldorf 40237, Germany

Prof. R. Schwaiger
Institute of Energy and Climate Research (IEK-2)
Forschungszentrum Juelich GmbH
Jülich 52425, Germany

Dr. B. Gault
Department of Materials
Imperial College London
Kensington, London SW7 2AZ, UK

The ORCID identification number(s) for the author(s) of this article can be found under https://doi.org/10.1002/smll.202004400.



**DOI: 10.1002/smll.202004400**

Multiple avenues are continuously being explored to fabricate new materials with intrinsic properties defying the physical limits of their predecessors. Over the past decades, nanocrystalline (NC) materials and metallic glasses (MG)[1] have been used for producing ever stronger materials. Hardening in NC exploits the resistance of interfaces against the motion of dislocations, which are the carriers of plastic deformation in crystals. This mechanism, referred to as the Hall–Petch effect,[2] below a critical grain size is no longer controlled by the motion of dislocations but by grain boundary sliding, resulting in softening.[3] In contrast, MG show excellent strength, yet, they usually undergo early catastrophic failure during yielding[4] because of the formation and propagation of shear bands. Glass–crystal (GC) nanocomposites offer the right blend of strength and plasticity,[5,6] but can be limited to thin-films, by size effects[7] and, compositionally, are restricted to a single amorphous phase. The next step in this evolution was the introduction of interfaces into glassy materials, an invention referred to as nanoglasses.[8,9] Their structure has been described to comprise nanosized glassy particles separated by interfaces of a different amorphous atomic structure and composition.[8,9] Nanoglasses fabricated by thermal evaporation inert gas condensation (IGC)[10] offer a wide range of possible compositions and can be synthesized in near-bulk sample sizes. IGC can produce sizes in the range of mm. However, the sizes are limited to the powder yield which is currently a few mg $h^{-1}$. Sc-Fe-based NG have shown enhanced plasticity compared to thin films or ribbons with similar compositions.[11] This was attributed to the glass-glass interfaces, which impede formation of large shear bands and instead trigger multiple smaller shear bands that dissipate the plastic energy better. Also, these materials show enhanced ferromagnetic properties compared to their ribbon counterparts.[12,13]

Here we develop this concept further by combining the nanoglass and the nanocrystal design concepts in form of a bulk Fe-10 at% Sc composite synthesized by IGC. Thermodynamic equilibrium for Fe-10 at% Sc suggests that pure Fe and an $Fe_2Sc$ intermetallic phase should actually coexist in such a compound after cooling. Correlative field ion microscopy (FIM) and atom probe tomography (APT), together with cryogenic-specimen preparation, reveal a highly complex state

with a nanoglass matrix consisting of amorphous grain-like units with near nominal composition (Fe-10 at% Sc), separated by glassy interfaces of different chemical composition which appear to be stabilized by hydrogen. This combined approach enabling chemistry-sensitive single-atom resolution characterization is essential here as the absence of larger symmetry units renders the real-space mapping of such complex nanochemical structures by other means practically impossible. The amorphous matrix grains contain pure-Fe nanocrystals and accompanied regions with a $Fe_2Sc$ stoichiometry, stemming from transient nanoscale partitioning. The cryogenic-specimen preparation also allows us to assess that the Sc-rich amorphous interfaces appear enriched by H, likely picked up during IGC.

This nanostructural and chemical hierarchy constitutes a new material class that we refer here to as nanoglass–nanocrystal composite. This novel alloy seems indeed to combine the advantages of glassy and nanocrystalline materials. It withstands a stress of 2.5 GPa before any inelastic yielding sets in, reaching a uniform deformation above 50% under compressive load at strengths above 6 GPa, a combination of mechanical features previously unattained by any other bulk material.[14] The structure changes during plastic deformation: the stiff Fe-rich nanocrystals are displaced in a rigid matter, carried by the slightly softer amorphous matrix, gradually agglomerating into nanocrystal clusters. While such a material design concept of blending nanoglasses with nanocrystals had been encouraged by simulation results,[15,16] no experimental realization had been previously demonstrated. It is also interesting to note that this complex hierarchy has been realized on such a compositionally simple binary alloy system as Fe-Sc.

We mapped the atomic-scale details of the structure and composition of the nanocomposite by combining APT and FIM, **Figure 1**. APT provides compositional mapping in 3D with sub-nanometer spatial resolution. Sets of isocomposition surfaces are shown in gold and cyan in Figure 1A highlighting Fe-rich and Sc-rich regions, while the 2D-compositional map of the Sc composition evidences the network of Sc-rich interfaces. We identified four distinct regions in the alloy: I) nanosized crystalline islands in the amorphous matrix grains which are enriched in Fe; II) a few nanosized islands enriched in Sc (directly adjacent to the Fe-rich regions) inside the amorphous matrix grains; III) well-defined amorphous interfaces, enriched in both Sc and H, that separate the amorphous matrix grains from each other; and IV) the amorphous matrix grains with a composition in Fe and Sc close to the nominal composition of the bulk material. More details from these APT atom map of these matrix and interfacial network regions are visible in Movie M1 (Supporting Information). A horizontal slice through the data showing all these features is shown in Figure 1B alongside a sketch of the structure. The composition profile plotted in Figure 1C corresponds to the region marked by an arrow in Figure 1A. The first island contains 100 at% Fe, while the adjacent Sc-rich region contains ≈70 at% Fe and 30 at% Sc. These compositions approach the compositions that would be expected for the two-phase region of the Fe-Sc equilibrium phase diagram[17] where 10 at% Sc addition leads to an Fe-rich bcc phase crystal and an $Fe_2Sc$

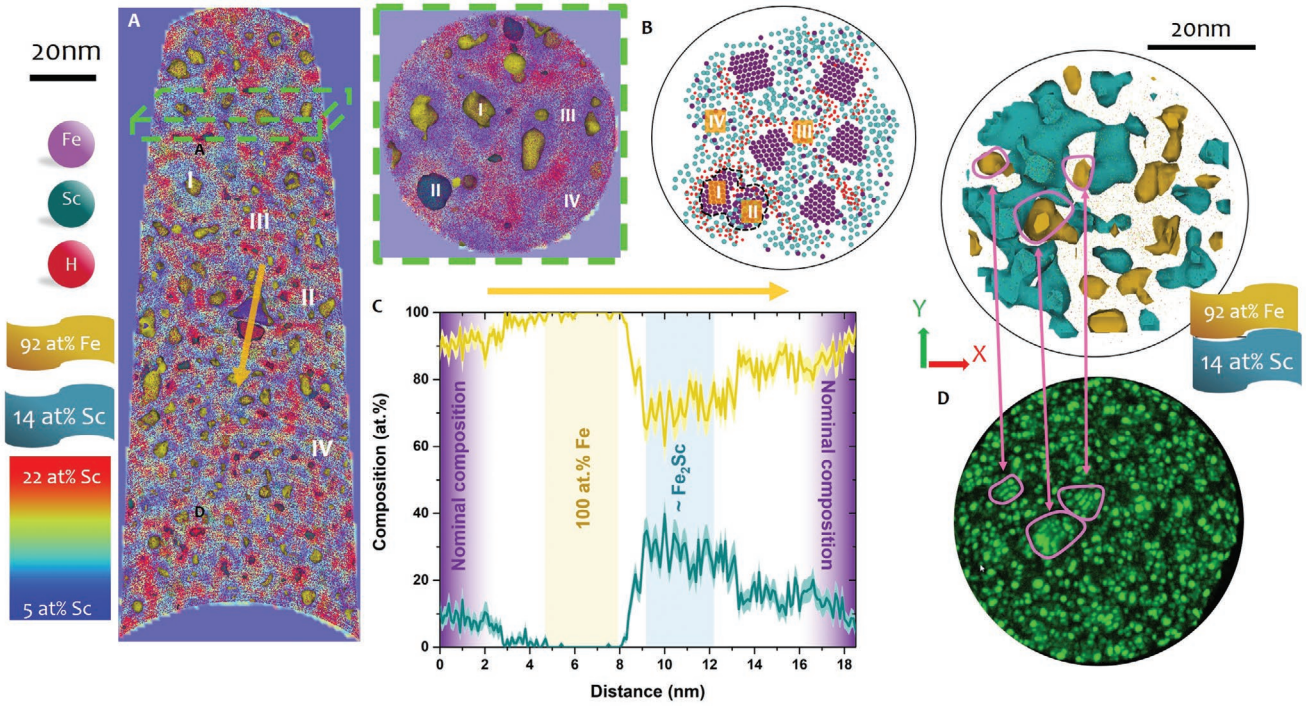


**Figure 1.** Correlative APT of the nanocomposite after an FIM analysis. A) Vertical 5 nm thick slice through an APT atom map, with isocomposition surfaces highlighting Fe- and Sc-rich regions, superimposed on a 2D compositional map of Sc. B) Horizontal 5 nm thick slice through the data and schematic model of the structure of the NGC. C) 1D composition profile along the yellow arrow in (A), traversing along IV–I–II–IV regions described in the text. D) 2D slice corresponding to the bottom of the APT data set and corresponding field-ion microscopy image confirming that Fe-rich regions are crystalline based upon the characteristic terraces, while the surrounding regions appear amorphous.

intermetallic phase in the moderate (300–1200 K) temperature regime.

After mapping the nanochemistry of the material the APT analysis was interrupted, and the specimen was imaged right away by FIM inside the same instrument. FIM offers true atomic resolution when imaging a material's surface, with the potential for observing crystalline defects such as dislocations and grain boundaries,[18,19] but does not readily offer compositional information. To combine these analytical capabilities, both techniques were performed on the same state-of-the-art instrument (see methods part for details). Figure 1D shows both a slice through the bottom section of the APT data and the corresponding FIM. We delineated in pink some of the Fe-rich islands highlighted by the set of gold-colored isosurfaces in the APT and their image in the field-ion micrograph. These Fe-rich islands exhibit the characteristic terraces and ledges related to the long-range periodic arrangement of atoms in a crystal and are hence crystalline in nature. Apart from these nanocrystals, the rest of the field-ion micrograph does not show any long-range periodicity and is effectively amorphous.

To summarize, Figure 1 allows us to confirm the proposed structure of a $Fe_{90}Sc_{10}$ nanoglass[20] that is made of nanoscale glassy grains and glassy interfacial regions. The glassy grains mostly contain an amorphous structure with a composition close to nominal, but some contain regions with a composition close to the $Fe_2Sc$ that are not imaged as crystalline by FIM and are hence likely amorphous. Interestingly, the interfacial region is enriched by ≈2 at% of hydrogen (Figure S1, Supporting Information). Cryogenic-specimen preparation was used to avoid H-contamination[21] and an analysis of the local variations in the electrostatic field rules out that the observed interfacial H-enrichment is an APT artifact[22] (Figure S2, Supporting Information). The FIM image of the Fe nanocrystals shows a bcc-compatible pole figure (Figure S3, Supporting Information). APT results obtained on the metallic glass reference material of the same composition, produced by melt spinning, are shown in Figure S4 (Supporting Information). This reference material shows no clusters or interface networks.

An analysis of the phase diagram indeed supports the assumption that there is a driving force for the nucleation of bcc-Fe nanocrystals. This would result in the rejection of Sc, which can lead to a partitioning of Sc out of the crystal and into the adjacent amorphous matrix. The Sc enrichment does however not yet lead to the formation of a $Fe_2Sc$ intermetallic phase, as would be expected from the phase diagram. Although the compositional enrichment is high enough, Figure 1D, at least directly adjacent to the Fe crystals, the two atomic species have to arrange into the ordered structure of the $Fe_2Sc$ intermetallic, which might be hindered by the high cooling rates and insufficient thermal activation. These partitioning and crystallization processes could i) either take place directly during the thermal evaporation of the constituents, and clusters of Fe-Sc with slight deviations from the glass forming composition could potentially undergo crystallization, i.e., a Sc deficiency would favor Fe-crystallization within the clusters; ii) or be promoted by an adiabatic temperature rise during compaction or exothermic reactions on the surface such as the absorption of, e.g., hydrogen or surface oxidation crystalline clusters during the IGC.

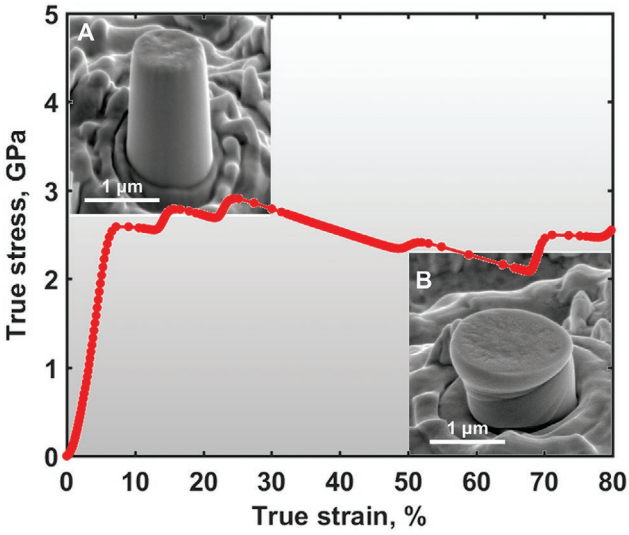


**Figure 2.** Micropillar compression and stress–strain behavior of the nanoglass–nanocrystal composite pillars. The true stress–strain curve reflects the formation and interaction of multiple shear bands, leading to a relatively homogeneous deformation. Inset A) Micropillar before compression. Inset B) Corresponding pillar after deformation.

Next, we evaluated the mechanical properties of the nanoglass–nanocrystal composite through micropillar compression testing using pillars with 1 µm diameter (**Figure 2**, inset A). The true stress–strain curve shows 2.5 GPa yield strength (Figure 2), one of the highest values ever observed for Fe-based alloys, including steels, and twice as high as that of a previously reported Sc-rich $Sc_{75}Fe_{25}$ nanoglass.[23] The addition of 10 at% Sc and our approach to nanostructuring by IGC leads to a 2.5–3 times increase in strength compared to pure iron micropillars.[24] Plastic deformation of the pillars shows a continuous stress increase interrupted by a series of load drops when deformed in load-control mode.[25] These load-drop regions mark the onset of multiple small shear bands which lead to a remarkably enhanced plasticity. Yet, we observe no pronounced strain localization leading to a catastrophic failure of the pillar even after ≈80% true strain (after which the test was stopped).

After deformation, the pillars show a pseudo-homogeneous deformation profile, Figure 2, inset (B), due to the activation and interaction of multiple shear bands, leading to a homogeneous increase of the diameter of the micropillar. This behavior contrasts with that of the fully amorphous metallic glass reference sample, where early failure immediately after yielding is generally observed,[7] with shear fracture typically along a 45–50° critically resolved shear stress plane as shown in Figure S5 (Supporting Information).

In order to examine the origin of the enhanced strength and plasticity, correlative FIM-APT was performed on the specimen deformed to 80% true strain. This is summarized in **Figure 3**. The four main constituents of the NGC are still present, including the Fe nanocrystals highlighted by the set of gold isocomposition surfaces in Figure 3A,B. The composition profile shown in Figure 3C indicates that the composition of the constituents has not changed significantly. The schematic shown in Figure 3D encapsulates the changes seen after deformation of the nanoglass–nanocrystal composite. Three

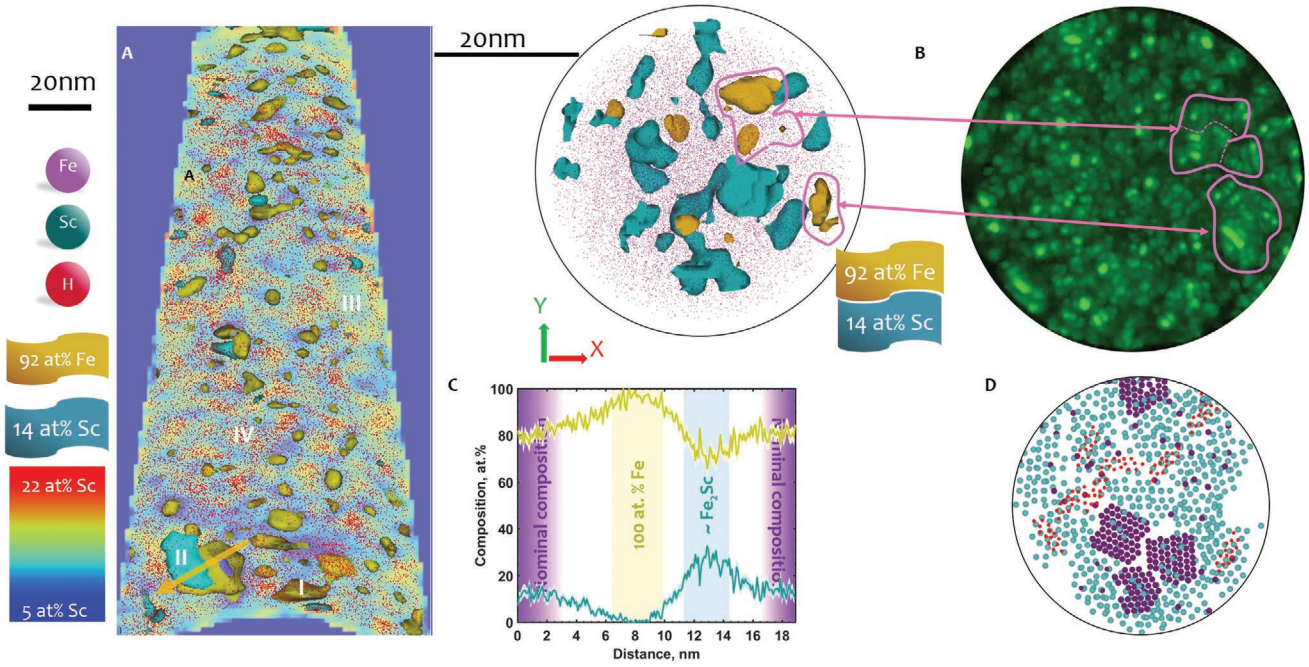


**Figure 3.** Correlative APT–FIM of the deformed nanoglass–nanocrystal composite. A) Vertical 5 nm thick slice through an APT atom map and iso-composition surfaces showing Fe- and Sc-rich regions and interfaces. B) Horizontal slice at the end of the APT data and corresponding FIM showing structural details of the crystalline Fe islands from the characteristic terraces produced in the FIM image and the amorphous surrounding regions are still apparent. The FIM image also indicates that the crystalline islands come in contact during deformation (separated by dashed pink lines). C) 1D composition profile along the orange arrow showing the 100% Fe in the nanocrystals. D) Sketch of the deformed NGC, drawn based on correlative observations.

important aspects arise. First, no clear elemental redistribution that would indicate mechanical induced mixing at the atomistic scale by the penetration by large shear bands[26] is detected by APT. Second, there is a slight loss of the clear crystalline pattern (Figure 3B) within the nanocrystals in FIM, yet, this feature is not accompanied by a change in their chemical composition. This may be indicative of deformation of the nanocrystals themselves. Third, the nanocrystals appear to agglomerate during deformation, when compared to the as-synthesized starting condition (Figure 3A,B), which could later lead to softening. A corresponding topological analysis of the nanocrystals is given in the Supporting Information, also revealing a gradual shape change of the crystals from spheres toward more disk-like objects. With ongoing deformation, larger agglomerates appear compared to the nondeformed state (Figure S7, Supporting Information).

Regarding the large plastic deformation, multiple shear bandings and quasi-homogeneous plastic flow likely take place in the amorphous parts. The glassy interfaces possibly also help enable quasi-homogeneous plastic flow.[3] While monolithic MGs show very limited inelastic deformation, plastic flow appears in sub-300 nm scale in the case of Sc rich nanoglass.[23] Size effects are not readily apparent in the current nanoglass–nanocrystal composite (Figure S8, Supporting Information). This mechanical behavior can be explained by following processes. High fraction of interfaces (glass-glass and glass-crystal) causes the facile nucleation of shear bands leading to the multiplication of shear bands, which prevents stress concentration or damage accumulation up to a critical level that would lead to failure. Further accumulation of the deformation leads to the agglomeration of the nanocrystals (as seen in Figure 3B, Figures S6 and S7, Supporting Information). Considering a simple rule of mixtures, it is apparent that the crystalline Fe (Young's modulus = 204 GPa) would stay largely intact while the Sc (Young's modulus = 74 GPa) rich surrounding regions tend to accommodate the deformation. This flow mechanism could bring the nondeforming Fe crystals in contact. This agglomeration can happen due to the interfacial network effectively blocking the free flow of Fe nanocrystals, ultimately enhancing yield strength to its near-theoretical limit.[6,27] The agglomeration of the crystals creates an effective size of the crystalline phase which could stop or slow down the propagation of shear bands. Ultimately, as the formation of larger shear bands is suppressed already at these extremely small length scales, a homogenous flow of the amorphous phase is plausible as also predicted by molecular dynamics simulations.[28] The improved plasticity arises due to the multiple shear bandings and homogeneous plastic flow in the nanoglass phase. Hints of dislocation activity in the crystalline phase are seen from contrast in FIM images, suggesting the deformation of crystals themselves. However, multiple interfaces and chemical variations make deconvolution of dislocation contrast difficult.

In summary, a bulk nanoglass–nanocrystal composite was fabricated and investigated at the true-atomic level revealing the complexity of its intrinsic structure and chemistry. The near-theoretical mechanical strength combined with high plasticity is direct consequences of the distribution of the nanoglass and nanocrystal phases, which allows circumventing the

strength–ductility tradeoff and any size effects. Such novel bulk materials have potential applications in areas where a combination of functional (such as magnetism) and extreme structural properties are in demand. The basic building and deformation principles of such novel nanoglass–nanocrystal composites revealed here, and the alloy design approach can also be extended to other alloy systems.

## Supporting Information

Supporting Information is available from the Wiley Online Library or from the author.

## Acknowledgements

Open access funding enabled and organized by Projekt DEAL.

## Conflict of Interest

The authors declare no conflict of interest.

## Keywords

correlative field ion and atom probe tomography, cryo-focused ion beam, high strength, nanoglass–nanocrystal composites, steel

Received: July 21, 2020
Published online: September 3, 2020

[1] A. L. Greer, in *Physical Metallurgy*, 5th ed. (Eds: D. E. Laughlin, K. Hono), Elsevier, Oxford **2014**, Vol. *1*, pp. 305–385.
[2] S. Yip, *Nature* **1998**, *391*, 532.
[3] J. Schiotz, *Science* **2003**, *301*, 1357.
[4] A. L. Greer, *Science* **1995**, *241*, 1640.
[5] G. Wu, K.-C. Chan, L. Zhu, L. Sun, J. Lu, *Nature* **2017**, *545*, 80.
[6] G. e. Wu, C. Liu, L. Sun, Q. Wang, B. Sun, B. Han, J.i-J. Kai, J. Luan, C. T. Liu, K.e Cao, Y. Lu, L. Cheng, J. Lu, *Nat. Commun.* **2019**, *10*, 5099.
[7] D. Jang, J. R. Greer, *Nat. Mater.* **2010**, *9*, 215.
[8] H. Gleiter, *Acta Mater.* **2008**, *56*, 5875.
[9] J. Jing, A. Krämer, R. Birringer, H. Gleiter, U. Gonser, *J. Non-Cryst. Solids* **1989**, *113*, 167.
[10] R. C. Flagan, M. M. Lunden, *Mater. Sci. Eng., A* **1995**, *204*, 113.
[11] X. L. Wang, F. Jiang, H. Hahn, J.u Li, H. Gleiter, J. Sun, J.i X. Fang, *Scr. Mater.* **2015**, *98*, 40.
[12] R. Witte, T. Feng, J. X. Fang, A. Fischer, M. Ghafari, R. Kruk, R. A. Brand, D. Wang, H. Hahn, H. Gleiter, *Appl. Phys. Lett.* **2013**, *103*, 073106.
[13] M. Ghafari, S. Kohara, H. Hahn, H. Gleiter, T. Feng, R. Witte, S. Kamali, *Appl. Phys. Lett.* **2012**, *100*, 133111.
[14] Y. Li, D. Raabe, M. Herbig, P. P. Choi, S. Goto, A. Kostka, H. Yarita, C. Borchers, R. Kirchheim, *Phys. Rev. Lett.* **2014**, *113*, 106104.
[15] W. R. Jian, L. Wang, X. H. Yao, S. N. Luo, *Nanotechnology* **2018**, *29*, 025701.
[16] C. Kalcher, O. Adjaoud, J. Rohrer, A. Stukowski, K. Albe, *Scr. Mater.* **2017**, *141*, 115.
[17] H. Okamoto, *J. Phase Equilib. Diffus.* **2012**, *33*, 80.
[18] D. G. Brandon, B. Ralph, S. Ranganathan, M. S. Wald, *Acta Metall.* **1964**, *12*, 813.
[19] G. D. W. Smith, D. Hudson, P. D. Styman, C. A. Williams, *Philos. Mag.* **2013**, *93*, 3726.
[20] C. Wang, X. Guo, Y. Ivanisenko, S. Goel, H. Nirschl, H. Gleiter, H. Hahn, *Scr. Mater.* **2017**, *139*, 9.
[21] Y. Chang, W. Lu, J. Guénolé, L. T. Stephenson, A. Szczpaniak, P. Kontis, A. K. Ackerman, F. F. Dear, I. Mouton, X. Zhong, S. Zhang, D. Dye, C. H. Liebscher, D. Ponge, S. Korte-Kerzel, D. Raabe, B. Gault, *Nat. Commun.* **2019**, *10*, 942.
[22] A. J. Breen, L. T. Stephenson, B. Sun, Y. Li, O. Kasian, D. Raabe, M. Herbig, B. Gault, *Acta Mater.* **2020**, *188*, 108.
[23] X. Wang, F. Jiang, H. Hahn, J.u Li, H. Gleiter, J. Sun, J. Fang, *Scr. Mater.* **2016**, *116*, 95.
[24] B. R. S. Rogne, C. Thaulow, *Philos. Mag.* **2015**, *95*, 1814.
[25] M. D. Uchic, *Science* **2004**, *305*, 986.
[26] S. Balachandran, J. Orava, M. Köhler, A. J. Breen, I. Kaban, D. Raabe, M. Herbig, *Scr. Mater.* **2019**, *168*, 14.
[27] R. L. Narayan, K. Boopathy, I. Sen, D. C. Hofmann, U. Ramamurty, *Scr. Mater.* **2010**, *63*, 768.
[28] T. Brink, K. Albe, *Acta Mater.* **2018**, *156*, 205.